Journal of Power Sources 270 (2014) 634–645

Contents lists available at ScienceDirect

Journal of Power Sources

journal homepage: www.elsevier.com/locate/jpowsour

Investigation of the electrospun carbon web as the catalyst layer for vanadium redox flow battery

Guanjie Wei, Xinzhuang Fan, Jianguo Liu*, Chuanwei Yan

Liaoning Engineering Research Center for Advanced Battery Materials, Institute of Metal Research, Chinese Academy of Sciences, Shenyang 110016, China

HIGHLIGHTS

- Vanadium reaction shows high reversibility on ECW.
- Conversion of carbon structure affects the electrochemical activity of ECW.
- Edge planes of graphitic lattice act as active sites for vanadium reaction.
- The ECW is used as catalyst layer for VRFB and improves its performance.

ARTICLE INFO

Article history:
Received 10 February 2014
Received in revised form
23 July 2014
Accepted 24 July 2014
Available online 1 August 2014

Keywords:
Electrospun carbon web
Polyacrylonitrile
Carbon nanofibers
Catalyst layer
Vanadium redox flow battery

ABSTRACT

Polyacrylonitrile (PAN) carbon nonwoven web consisting of 100–200 nm ultrafine fibers has been developed by electrospinning and subsequent carbonization process at 1000 °C for different times. The surface morphology, composition, structure, and electrical conductivity of the electrospun carbon webs (ECWs) as well as their electrochemical properties toward vanadium redox couples have been characterized. With the increasing of carbonization time, the electrochemical reversibility of the vanadium redox couples on the ECW is enhanced greatly. As the carbonization time increases up to 120 min, the hydrogen evolution is facilitated while the reversibility is promoted a little bit further. The excellent performance of ECW may be attributed to the conversion of fibers carbon structure and improvement of electrical conductivity. Due to the good electrochemical activity and freestanding 3-dimensional structure, the ECW carbonized for 90 min is used as catalyst layer in vanadium redox flow battery (VRFB) and enhances the cell performance.

1. Introduction

The VRFB has recently received considerable attentions as a large scale energy storage system for intermittent renewable energy (such as solar and wind energy, etc.) due to its outstanding properties such as long cycle life, high reliability, flexible design and environmental friendliness [1–3]. The VRFB employs VO^{2+}/VO_2^+ and V^{2+}/V^{3+} redox couples as positive and negative half cell, respectively. Its open circuit voltage is approximately 1.26 V at 100% stage of charge [4,5]. Due to ions of the same chemical element are used in both half cells, the common problem of cross-contamination in other redox flow battery does not appear in VRFB. As an important part of VRFB, the electrode supplies the redox reaction with places and facilitates the reaction. Therefore, an ideal electrode should possess high electrochemical activity, high electrical conductivity, large surface area, appropriate wettability and stability in the concentrated acid solution. Up to now, carbon based materials especially PAN-based carbon felt (CF) or graphite felt are practically used in VRFB because of their large surface area, large porosity, high electrical conductivity and low cost. However, due to the poor kinetics and reversibility of the vanadium redox couples on these materials, the energy efficiency (EE) of VRFB is limited greatly. Therefore, considerable efforts have been devoted to enhance their electrochemical activity. The most common methods include thermal treatment, acid oxidation and active material modification [6–9], while these methods just focus on the activity of the surface function groups (oxygen or nitrogen function groups) and the effect of surface area, influence of carbon structure on the electrochemical performance of the PAN-based carbon fibers is in lack of investigation.

Nowadays, electrospinning has been adopted as an efficient approach to prepare nanofibers and high surface area fibrous web.

* Corresponding author. Tel.: +86 24 2399 8320; fax: +86 24 2388 0201.
E-mail addresses: jgliu@imr.ac.cn, jt32123@163.com (J. Liu).

http://dx.doi.org/10.1016/j.jpowsour.2014.07.161
0378-7753/

With this technique and subsequent carbonization process, PAN polymer and its composite can be easily made into carbon nanofibers (CNFs) or carbon fibrous web [10–13]. By controlling the preparation process, PAN-based CNFs with different morphology, composition and structure can be obtained and their structure–function relationship can be studied systematically. Furthermore, because the electrospun CNFs are generally prepared in the form of nonwoven web, it can be used as electrode catalyst without any binder, which brings more convenience to its application in VRFB. Based on the reasons mentioned above, the PAN-based ECW consisting of nanofibers has been developed in our previous work and the effect of carbonization temperature on the ECW also has been investigated. It is found that electrochemical properties of the ECW really depend on the carbon structure and the electrical conductivity [14]. In order to further study the effect of carbon structure on the electrochemical activity of the PAN-based carbon fibers, the ECW was carbonized at 1000 °C for different times in this research. The conversion of carbon structure and improvement of electrical conductivity relating to the carbonization time were studied, and their effects on the electrochemical properties were also investigated. Besides, the ECW was used as catalyst layer in VRFB practically by two approaches. Cyclic voltammetry (CV) measurement and single cell test demonstrated the effect of ECW introduction.

2. Experimental

2.1. Preparation of the ECW and ECW/CF composite electrode

Electrospun nonwoven web consisting of nanofibers was prepared by the process reported in the previous work [14]. Then the web was pre-oxidized at 280 °C for 30 min in air. After that, the stabilized web was carbonized by heating them to 1000 °C at a rate of 5 °C min^{-1} and holding for 30 min, 60 min, 90 min and 120 min in nitrogen flow. For the prepared samples, the ECW carbonized for different times are denoted as 30 min-ECW, 60 min-ECW, 90 min-ECW, 120 min-ECW, respectively. The thickness of ECW is about 30 μm.

The PAN-based CF (thickness: 4–5 mm) as pristine CF bought from Shenhe carbon fiber Materials Co. Ltd was cut into piece of 4 cm × 9 cm. Then, the CF was fixed on the roller and acted as collector for the electrospun nonwoven web. After the web was spun on one side of the CF, the composite was pre-oxidized at 280 °C for 30 min in air. Next, the stabilized composite was carbonized by heating up to 1000 °C at a rate of 5 °C min^{-1} and holding for 90 min in nitrogen flow. After this process, the ECW/CF composite electrode was obtained. For comparing, the CF without the ECW was also treated by the same carbonization process, which was denoted as 1000 °C-1.5 h CF.

2.2. Materials characterizations

The surface morphology and diameter distribution of the ECW were examined by scanning electron microscopy (SEM). The surface elements and functional groups were analyzed by X-ray photoelectron spectroscopy (XPS). All binding energy values were calibrated to the C1s graphitic peak at 284.7 eV. The conversion of carbon structure was reflected by X-ray diffraction (XRD) and transmission electron microscopy (TEM). The electrical conductivity of the ECW was measured by the four-probe method.

2.3. Electrochemical measurement

For electrochemical measurement, a three-electrode cell was used with a piece of ECW or ECW/CF composite as the working electrode, a saturated calomel electrode as the reference electrode, and a Pt electrode as the counter electrode. The working electrode was sandwiched between a rubber sheet and a Ti plate. The sheet had a hole as the working area (hole area of 0.283 cm^2 for the ECW, hole area of 1 cm^2 for the ECW/CF composite), and the Ti plate contacting the working electrode directly acted as current collector. The schematic diagram of the three-electrode cell is shown in Fig. 1.

The electrochemical property of the working electrode was tested by CV and electrochemical impedance spectra (EIS) measurement. The CV curves were recorded in 0.1 M $VOSO_4$ + 2.0 M H_2SO_4 solution. The EIS was measured by applying an alternating voltage of 5 mV over the frequency ranging from 10^5 to 10^{-2} Hz in 0.1 M VO^{2+} + 2.0 M H_2SO_4 and 0.1 M V^{3+} + 2.0 M H_2SO_4 solution, respectively.

2.4. VRFB single cell test

The constant current charge and discharge test was carried out using a VRFB single cell. As for the cell structure, which is shown in Fig. 2, the conductive plastic plates were used as current collectors and Nafion 212 ion exchange membrane served as the separator. Pristine CF (Size: 4 cm × 7 cm) acted as substrate of the electrodes for both half cells and the active area of each electrode was 28 cm^2. The cell was sealed with rubber washers. The initial electrolytes for both positive and negative half cell were 1.2 M $VOSO_4$ + 3.0 M H_2SO_4, and the volume of negative electrolyte was 80 mL while that of the positive one was 160 mL to obtain balanced charge capacity. The electrolyte was pumped into the cell and cycled at a fixed speed during the cell test.

The 90 min-ECW was applied as catalyst layer in the cell with two methods. One was using ECW/CF composite to replace pristine CF as electrode, and the ECW contacted with the ion exchange membrane. The other method was directly sandwiching the ECW (Size: 2 cm × 3 cm) between pristine CF electrode and ion exchange membrane as catalyst layer in both half cells. The upper limit of charge voltage and the lower limit of discharge voltage were controlled to be 1.65 and 0.75 V vs. SCE, respectively, in order to avoid over-charging the battery.

3. Results and discussion

3.1. Morphology and composition of the ECW

The morphologies of the ECWs carbonized for different times are presented in Fig. 3. With the increasing of carbonization time, diameters of the CNFs change rarely, which are mainly distributed

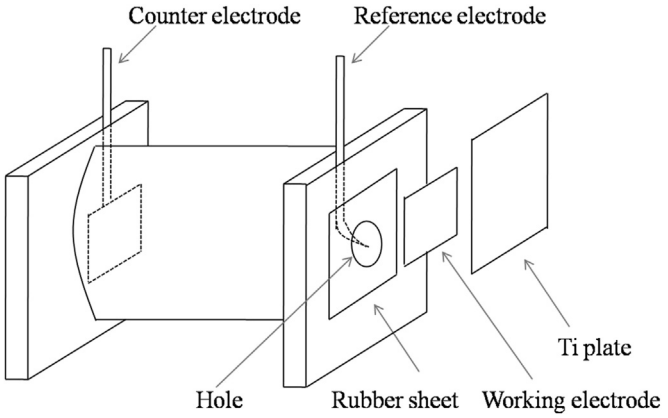

Fig. 1. Schematic diagram of the three-electrode cell.

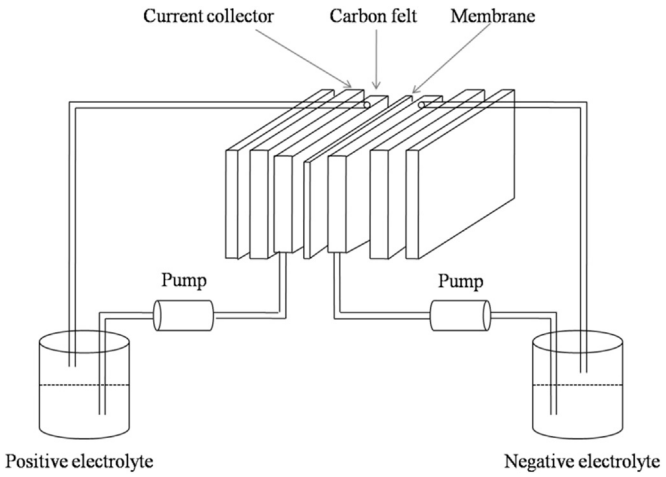

Fig. 2. Schematic diagram of the VRFB single cell.

with the range of 100–200 nm. Besides, cross section of the 90 min-ECW showed in Fig. 3e indicates the CNFs have a solid core structure. The compositions of the ECWs carbonized for different times are analyzed by XPS. Fig. 4 illustrates the evolution of the elements and their relative functional groups. The elements of ECW are mainly carbon, nitrogen, and oxygen, and the content of which does not change significantly as the carbonization time increases. As listed in Table 1, the carbon content is 91–93 at.%, both of the oxygen and nitrogen contents are 3–5 at.%. From the curve-fitted N1s high-resolution XPS of the ECW, four types of nitrogen functional groups are found, which correspond to pyridinic nitrogen (398.0–398.2 eV), pyrrolic nitrogen (399.1–399.8 eV), graphitic nitrogen (400.2–400.9 eV) and pyridine-N-oxide (around 402.0 eV), respectively [15,16]. From Fig. 4b, it can be seen clearly that with the increasing of carbonization time, the content of pyridinic nitrogen decreases and that of graphitic nitrogen increases accordingly, while both of the changes are quite small. As for the oxygen functional groups, the O1s high-resolution XPS reveals the presence of three peaks. They are attributed to the C=O groups in ketone, lactone or carbonyl (530.8–531.1 eV), C–O groups in hydroxyls or ethers (531.7–532.3 eV) and chemisorbed oxygen or oxygen atoms in adsorbed water (533.1–533.5 eV) [17,18]. Not like the conversion of nitrogen functional groups at different carbonization times, the content of the oxygen functional groups for each type remains more or less constant. For all of the samples, the C=O groups occupy the main quantity. Compared with the carbonization temperature, influence of the carbonization time on the evolution of composition of the PAN carbon fibers is slight [14,19,20].

3.2. Carbon structure and electrical conductivity of the ECW

The XRD patterns in Fig. 5 reflect the carbon structures of the ECWs carbonized for different times. With the increasing of carbonization time, the (002) diffraction peak of ECW located around 25° becomes sharper and shifts toward higher 2θ, indicating the graphitization degree of ECW improves. The *c*-axis spacing (d_{002}) and crystallite size (Lc) of the ECW calculated from the Bragg equation and Scherrer's formula are listed in Table 2. The d_{002} values of the ECWs are much larger than that of graphite (0.335 nm), implying the microstructure of ECW is a turbostratic carbon structure [19,21]. As the carbonization time is extended, the d_{002} value decreases and the Lc increases little by little, demonstrating the graphite layers in turbostratic carbon structure become ordered and the graphitization degree of ECW is promoted.

In order to examine the microstructure of CNFs in ECW visually, TEM images of ECWs are obtained. Fig. 6 shows the morphology of individual CNFs in the 90 min-ECW. The surface of CNFs is rough and looks like undulating waves. In the high-resolution TEM image of the CNFs, a series of lattice fringes corresponding to (002) planes are generally parallel to the fiber axis in the skin region [21,22]. The d_{002} value obtained from the image shows good agreement with the value from Bragg equation. Fig. 7 presents the high-resolution TEM images of the CNFs carbonized for different times further. With the increase of carbonization time, stacking thickness of the (002) planes aligned along the fiber axis increases. The result is in keeping with the changes of graphitization degree. Fig. 8 shows electrical conductivity of ECW. The relative data are listed in Table 3. With the increasing of carbonization time, electrical conductivity of the ECW improves sharply. This may be attributed to the increasing 2-dimensional graphitic lattice with a preferred orientation in parallel to the fiber axis and the promoted ordering of the turbostratic carbon structure [20,23].

3.3. Electrochemical properties of the ECW

3.3.1. CV measurement

As illustrated in Fig. 9, CV behaviors of the ECWs carbonized for different times were investigated at scan rate of 2 mV s^{-1} in the electrolyte containing 0.1 M $VOSO_4$ and 2.0 M H_2SO_4. The electrochemical parameters for VO^{2+}/VO_2^+ and V^{3+}/V^{2+} redox couples are listed in Tables 4 and 5. For all samples, the voltammogram shows two couples of peaks obviously which correspond to the VO^{2+}/VO_2^+ and V^{2+}/V^{3+} redox reaction, respectively. In the case of the 30 min-ECW, VO^{2+}/VO_2^+ or V^{2+}/V^{3+} redox couple shows extremely large peak potential separation (ΔEp) and asymmetric peak shape, indicating the electrochemical activity is very poor. With the increasing of carbonization time, the electrochemical reversibility of the redox couples becomes better, since the samples have smaller ΔEp accompanied by a ratio of peak current (Ipa/Ipc) closed to unity. However, as the carbonization time increases to 120 min, the increase extent of the reversibility for two redox couples becomes marginal and the hydrogen evolution is facilitated.

Fig. 10 presents the CV curves of the ECWs carbonized for different times recorded at different scan rates. The relative ΔEp values are listed in Table 6. For each sample, the ΔEp values of two redox couples increase with the scan rate and the increase extent reflects different polarization. As for the VO^{2+}/VO_2^+ redox couple, when the scan rate increases from 2 to 20 mV s^{-1}, the increase of ΔEp value for 60 min-ECW, 90 min-ECW and 120 min-ECW is 614 mV, 370 mV and 338 mV, respectively. For the V^{2+}/V^{3+} redox couple, the corresponding increase of ΔEp is 388 mV, 320 mV, 270 mV, respectively. It indicates the polarization of redox reaction on the ECW reduces with the increase of carbonization time. This may be attributed to the increasing electrical conductivity of the ECW [24,25]. As given in Fig. 11, the peak current of VO^{2+}/VO_2^+ and V^{2+}/V^{3+} redox couple prove to be proportional to the square root of the scan rate on the 60 min-ECW, 90 min-ECW and 120 min-ECW. It provides evidence that the oxidation and reduction behaviors of the two redox couples on these ECWs are controlled by diffusive mass transport [26]. The slope of 90 min-ECW is larger than that of 60 min-ECW and 120 min-ECW, suggesting a faster mass transport process on the 90 min-ECW [27,28].

3.3.2. EIS analysis

In order to further analyze the cause of the increasing electrochemical activity, EIS of the VO^{2+}/VO_2^+ and V^{2+}/V^{3+} redox couple on ECWs carbonized for different times were recorded at different potentials. Fig. 12a shows the Nyquist plots of VO^{2+}/VO_2^+ redox

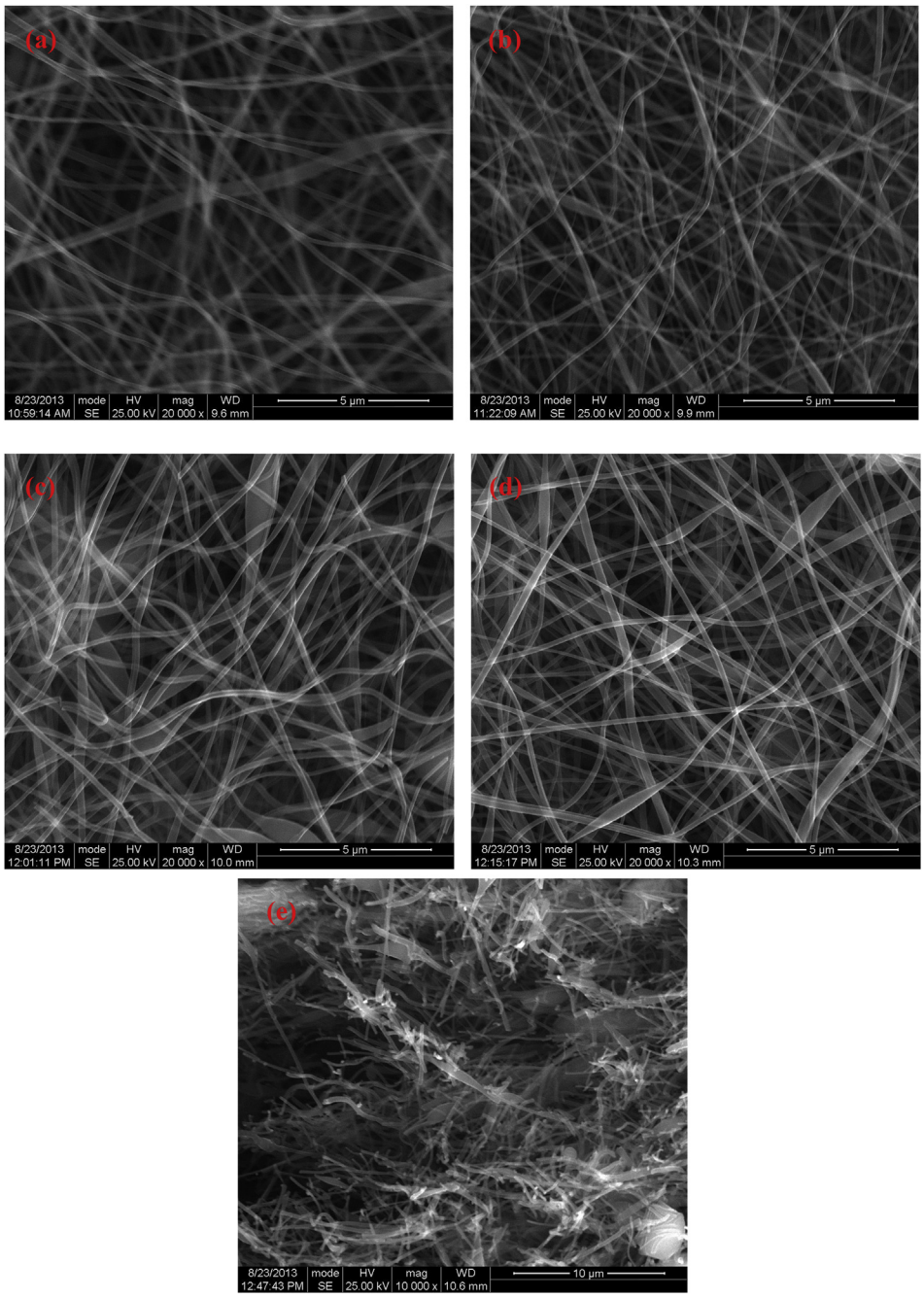

Fig. 3. SEM images of the ECWs carbonized for different times: Surface morphology of the 30 min-ECW (a), 60 min-ECW (b), 90 min-ECW (c), and 120 min-ECW (d); cross-section of the 90 min-ECW (e).

couple recorded at the polarization potential of 0.9 V in the electrolyte containing 0.1 M VO^{2+} and 2.0 M H_2SO_4, while Fig. 12b shows the Nyquist plots of V^{2+}/V^{3+} redox couple recorded at the polarization potential of −0.6 V in the electrolyte containing 0.1 M V^{3+} and 2.0 M H_2SO_4. For all samples, the Nyquist plots consist of two semicircles and a linear part in the frequency range from 10^5 to 10^{-2} Hz at the polarization potential. Thus, the Nyquist plots can be fitted with equivalent circuit in Fig. 12c. Rs stands for the ohmic solution resistance; CPE1 and Rc represent the capacitance and resistance arisen between the fibers as well as between the ECW and electrolyte; CPE2 and Rct represent the electric double-layer capacitance of electrode/solution interface and charge transfer resistance across the interface, respectively; CPE3 represents the diffusion capacitance attributed by the diffusion process of vanadium ions [8,29].

The parameters obtained from fitting the impedance plots with the equivalent circuit in Fig. 12 are listed in Table 7. According to the fitting result, the Rs values for all samples nearly remain constant in the given electrolyte, and the average value is 4.5 Ω. With the consideration of that the contact resistances between ECW and electrolyte is identical, the decrease in Rc value with the increase of carbonization time indicates a reduction of the ECW resistance, which shows good agreement with the improved electrical conductivity of ECW. With the increasing of carbonization time, the Rct values for VO^{2+}/VO_2^+ and V^{2+}/V^{3+} redox reaction reduce, suggesting the electron transfer kinetics is enhanced. As the

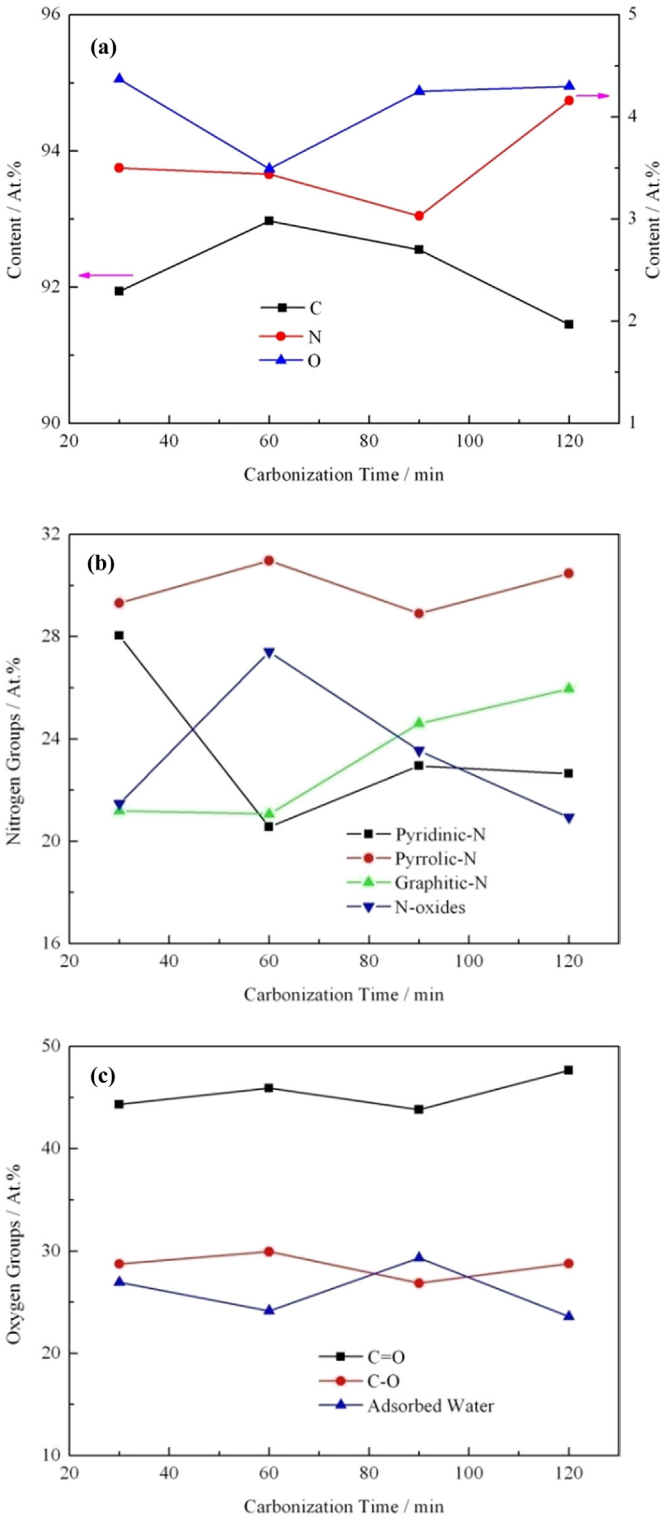

Fig. 4. XPS analysis of the ECWs carbonized for different times: (a) change of the elements content, (b) evolution of the nitrogen functional groups, (c) evolution of the oxygen functional groups.

carbonization time is extended to 120 min, the decrease extent of Rct value is slight. In the equivalent circuit, CPE3 (expressed as $CPE = Y_0^{-1}(jw)^{-n}$) reflects the diffusion process of vanadium ions, and an increase in the prefactor Y_0 implies a decrease of the diffusion impedance. For the VO^{2+}/VO_2^+ redox couple, magnitude

Table 1
Elements content of the ECWs carbonized for different times.

Elements	30 min (%)	60 min (%)	90 min (%)	120 min (%)
C	91.94	92.97	92.55	91.45
N	3.50	3.44	3.03	4.16
O	4.37	3.49	4.25	4.30
S	0.18	0.10	0.18	0.09

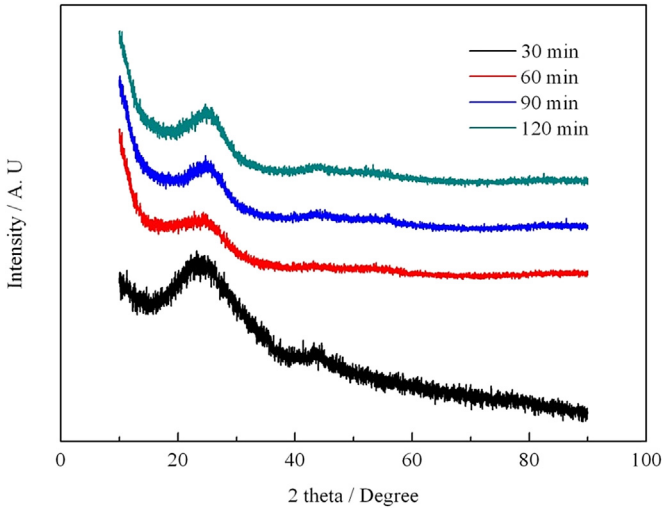

Fig. 5. XRD patterns of the ECWs carbonized for different times.

Table 2
Parameters obtained from XRD pattern of the ECWs carbonized for different times.

Carbonization time (min)	$d_{(002)}$ (nm)	Lc (nm)
30	0.375	1.0
60	0.366	1.6
90	0.358	2.0
120	0.358	1.8

of Y_0 for the 60 min-ECW, 90 min-ECW and 120 min-ECW is 0.074, 0.28, and 0.23, respectively. For the V^{2+}/V^{3+} redox couple, the corresponding value is 0.0056, 0.14, and 0.062, respectively. Obviously, the 90 min-ECW possesses the largest Y_0 value, indicating the mass transport rate of the vanadium ions through pore channel of the ECW is the highest. The results are also consistent with the CV measurement.

Taken all together, when the carbonization time increases from 30 min to 90 min, enhancement of the electrochemical activity of ECW is large. However, as the carbonization time increases from 90 min to 120 min further, the increase extent of electrochemical activity reduces. Taking account of the electrode reaction process, the results mentioned above demonstrate the increasing electrochemical activity of the ECW could be attributed to the improvement in electron transfer kinetics and mass transport rate [28,30]. With the increasing of the carbonization time, morphology and composition of the ECW have not changed significantly while the carbon structure transforms a lot. There are two big changes happening to the carbon structure with the increase of the carbonization time. In one aspect, there are more 2-dimensional graphitic lattices forming in the CNFs and the stacking of graphitic layers increases; in the other aspect, the amount of graphitic layers interconnect and extend, thus, the broadness and orientation of the 2-dimensional graphitic lattice in the direction of fiber axis is improved [31]. As shown in Table 2, when the

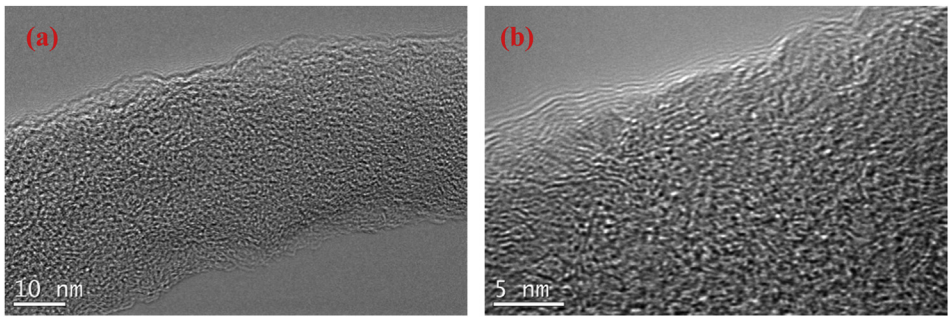

Fig. 6. TEM images of CNFs in the 90 min-ECW: (a) microstructure of the nanofibers at low resolution, (b) microstructure of the nanofibers at high resolution.

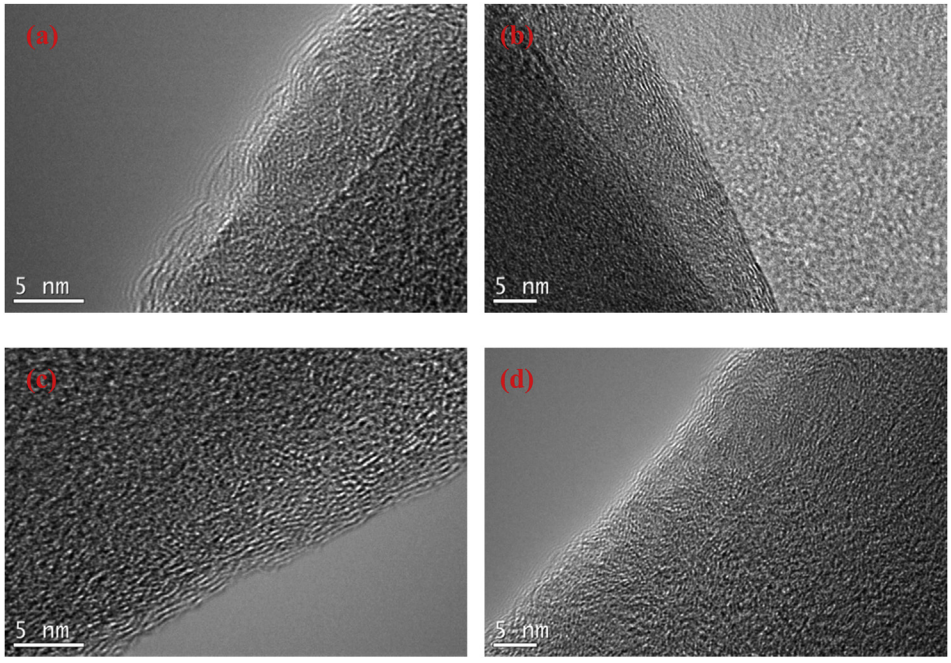

Fig. 7. Microstructure of CNFs at high resolution in the 30 min-ECW (a), 60 min-ECW (b), 90 min-ECW (c), and 120 min-ECW (d).

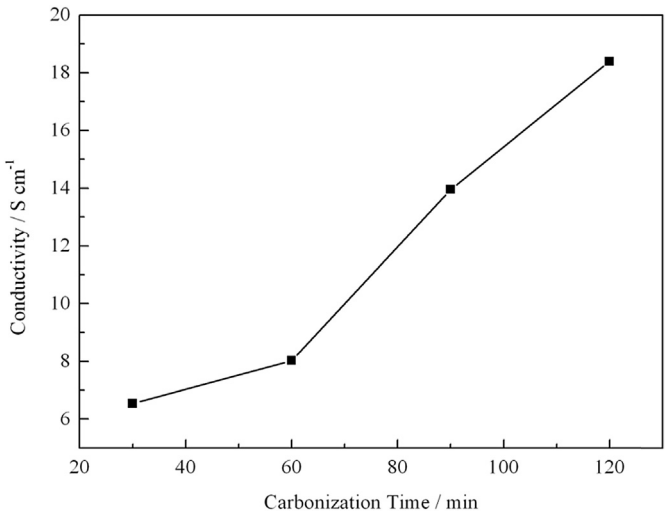

Fig. 8. Effect of the carbonization time on the electrical conductivity of ECW.

carbonization time increases from 30 min to 90 min, stacking of the graphitic layers mainly arises in the carbon fibers. Not only do the graphitic layers contribute to promote the electrical conductivity of carbon fibers, but also the abundant exposed carbon edge planes act as active sites for vanadium ions adoption [30]. Therefore, the electron transfer kinetics and mass transport rate are improved at the same time. However, as the carbonization time increases from 90 min to 120 min, stacking of the graphitic layers is not enlarged further while the interconnection of them mainly arises, resulting in a reduction of the carbon edge planes quantity. Thus, although the electron transfer kinetics can be further promoted because of the enhanced electrical conductivity, the mass transport rate is reduced due to the decrease of edge planes quantity [32]. Hence, the electrochemical activity of the ECW was enhanced a little as the carbonization time increases to 120 min. As a result of analysis, the increasing performance of ECW has a closed relationship with the conversion of fibers carbon structure as well as the resulting provision of higher electrical conductivity.

Table 3
Electrical conductivities of the ECWs carbonized for different times.

Carbonization time (min)	30	60	90	120
Conductivity (S cm^{-1})	6.54	8.02	14.0	18.4

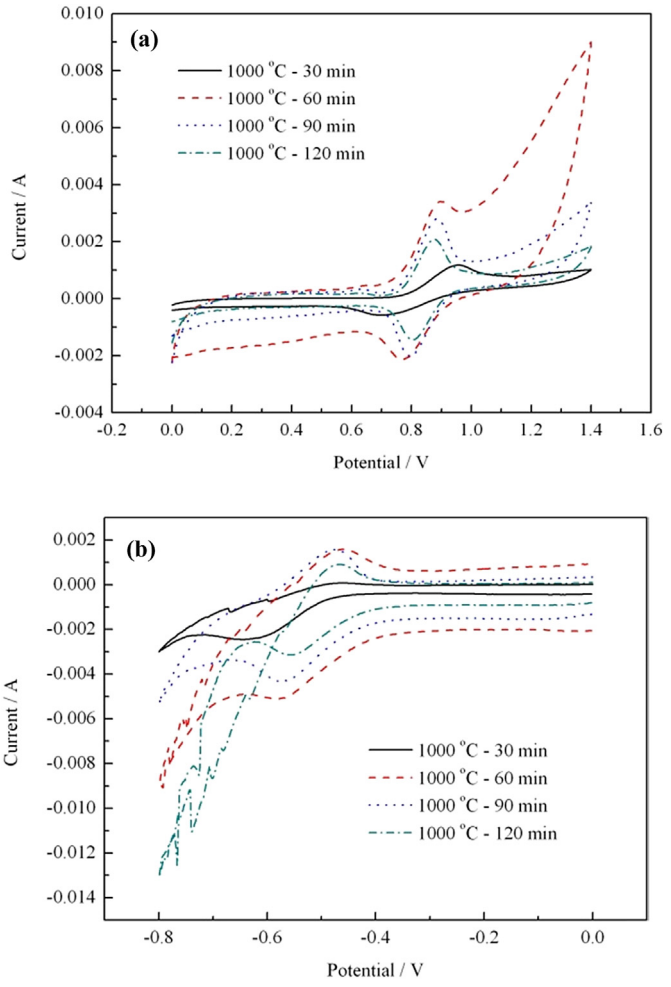

Fig. 9. CV curves for VO^{2+}/VO_2^+ (a) and V^{2+}/V^{3+} redox couple (b) on the ECWs carbonized for different times recorded at 2 mV s^{-1} scan rate in 0.1 M $VOSO_4$ + 2.0 M H_2SO_4.

3.4. Morphology and CV behavior of the ECW/CF composite electrode

Due to the good electrochemical activity and freestanding 3-dimensional structure, the 90 min-ECW was spun onto the CF electrode as catalyst layer. Fig. 13 illustrates SEM images of the ECW/CF composite electrode. As shown in Fig. 13a, diameter of the carbon fibers in the CF is about 20 μm while that of the CNFs is in range of 100–200 nm. Fig. 13b shows the orientation of CNFs is very high, which may be affected by the knitting direction of carbon fibers in the CF. From the cross-section of ECW/CF composite

Table 4
Parameters recorded by the CV curves for VO^{2+}/VO_2^+ couple on the ECWs carbonized for different times.

Carbonization time (min)	Ipa (mA)	Ipc (mA)	−Ipa/Ipc	Ea (V)	Ec (V)	ΔEp (V)
30	1.17	−0.584	2.00	0.958	0.694	0.264
60	3.41	−2.14	1.59	0.898	0.772	0.126
90	2.81	−2.02	1.39	0.886	0.796	0.09
120	2.1	−1.45	1.45	0.878	0.802	0.076

Table 5
Parameters recorded by the CV curves for V^{2+}/V^{3+} couple on the ECWs carbonized for different times.

Carbonization time (min)	Ipa (mA)	Ipc (mA)	−Ipa/Ipc	Ea (V)	Ec (V)	ΔEp (V)
30	0.0723	−2.46	0.03	−0.46	−0.646	0.186
60	1.58	−5.11	0.31	−0.462	−0.582	0.12
90	1.56	−4.32	0.36	−0.474	−0.574	0.1
120	0.903	−3.14	0.29	−0.464	−0.558	0.094

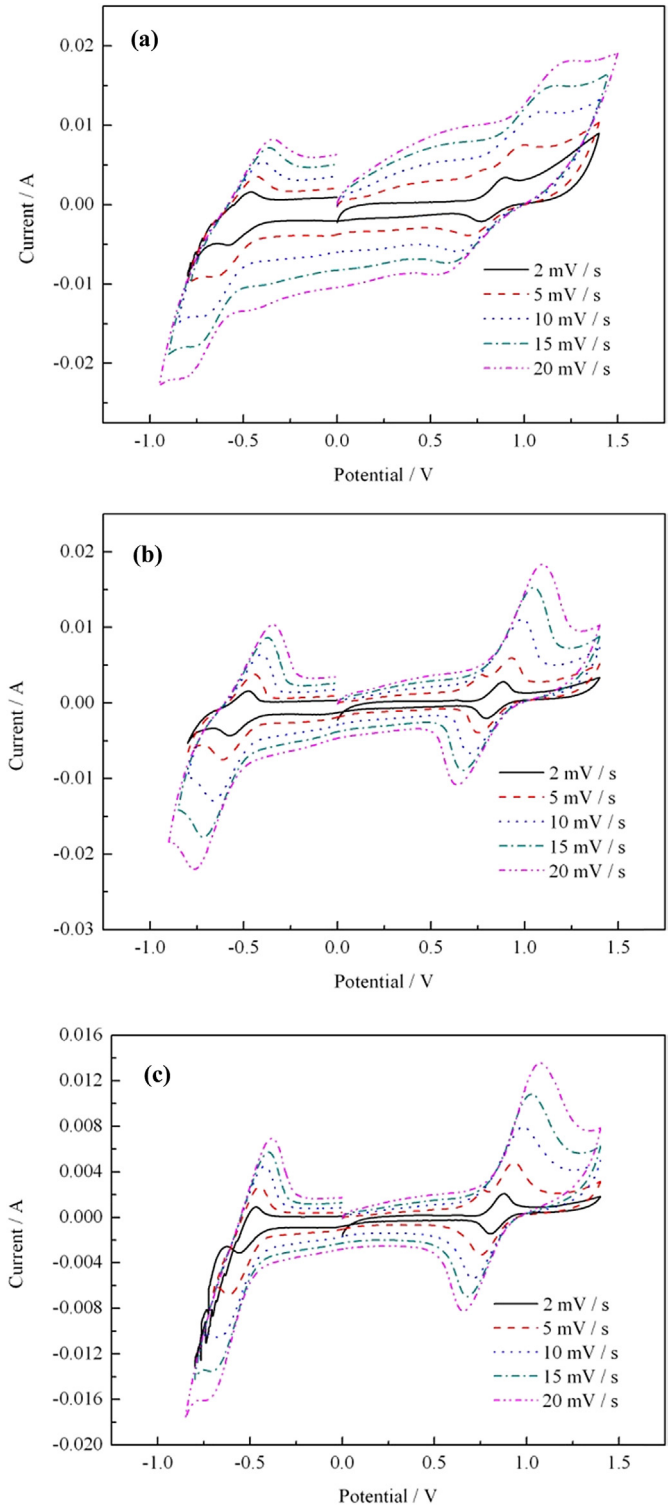

Fig. 10. CV curves for vanadium redox couples on 60 min-ECW (a), 90 min-ECW (b), and 120 min-ECW (c) recorded at different scan rates in 0.1 M $VOSO_4$ + 2.0 M H_2SO_4.

Table 6
ΔEp values obtained from CV curves recorded at different scan rates for vanadium redox couples on the ECWs carbonized for different times.

Scan rate (mV s^{-1})	Positive ΔEp (mV)			Negative ΔEp (mV)		
	60 min	90 min	120 min	60 min	90 min	120 min
2	126	90	76	120	100	94
5	298	174	188	234	168	174
10	448	282	276	330	262	252
15	586	380	352	420	344	312
20	740	460	414	508	420	364

electrode (Fig. 13c), it can be seen the ECW is ultrathin and some parts of ECW have been damaged during the subsequent carbonization process. These two aspects are bad for the performance of ECW and the loading method of ECW on the CF needs to be further optimized.

Fig. 14 presents the CV curves of VO^{2+}/VO_2^+ and V^{2+}/V^{3+} redox couple on the ECW/CF composite electrode. For comparing, the pristine CF and 1000 °C-1.5 h CF were also analyzed. As shown in Tables 8 and 9, ΔEp for the VO^{2+}/VO_2^+ redox couple is larger than that of the V^{2+}/V^{3+} redox couple on pristine CF, indicating the redox reaction rate of the former is faster than that of the latter. Compared

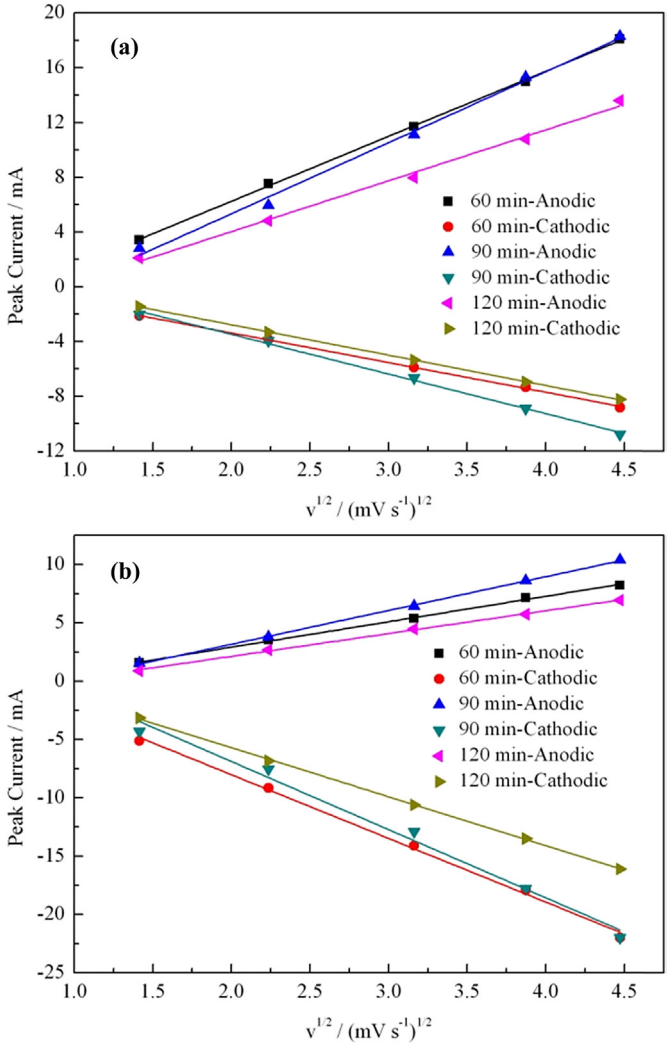

Fig. 11. Peak current as a function of square of scan rate on the ECWs carbonized for different times for VO^{2+}/VO_2^+ (a) and V^{2+}/V^{3+} redox couple (b).

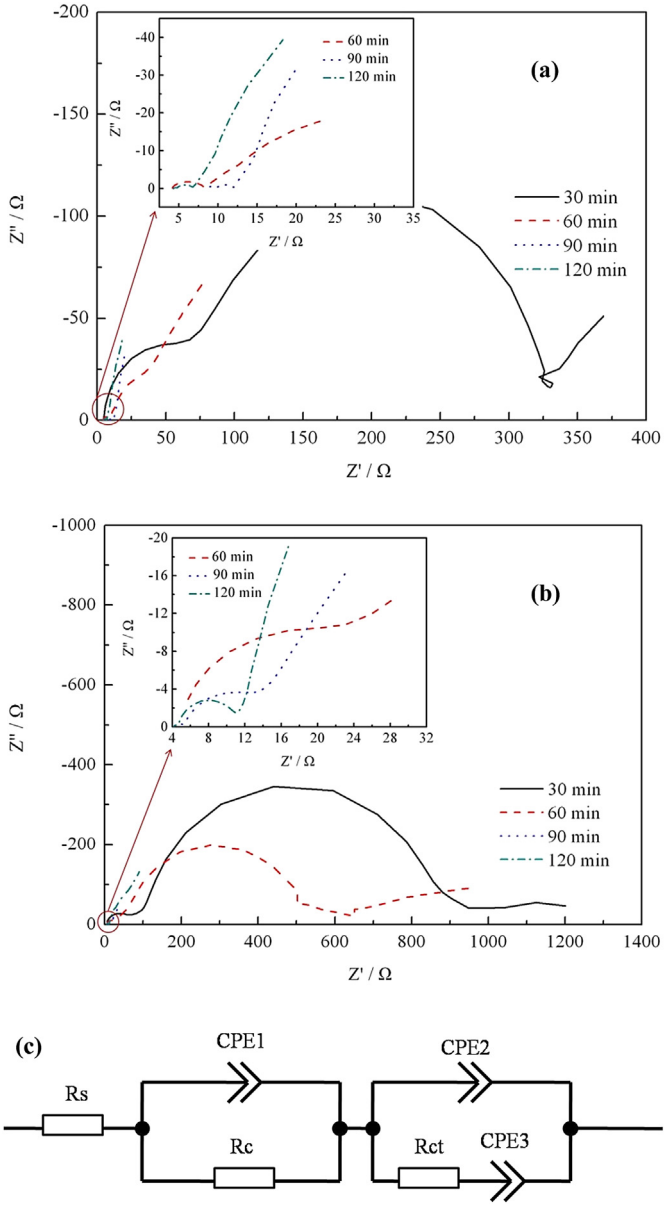

Fig. 12. Nyquist plots and the corresponding equivalent circuit of the ECWs carbonized for different times for vanadium redox couples at different potentials: (a) VO^{2+}/VO_2^+ redox couple at the polarization potential of 0.9 V, (b) V^{2+}/V^{3+} redox couple at the polarization potential of −0.6 V, (c) equivalent circuit for the electrode process.

with the pristine CF, ΔEp on the ECW/CF composite electrode is reduced a lot for two redox couples, especially for the V^{2+}/V^{3+} redox couple, while ΔEp on the 1000 °C-1.5 h CF changes a little. Moreover, the reaction current of the ECW/CF composite electrode

Table 7
Parameters obtained from fitting the impedance plots at polarization potential with the equivalent circuit of ECWs carbonized for different times.

Carbonization time (min)	Positive			Negative		
	Rs (Ω)	Rc (Ω)	Rct (Ω)	Rs (Ω)	Rc (Ω)	Rct (Ω)
30	4.66	62.5	260	3.33	81.8	803
60	4.20	4.02	53.2	1.71	53.5	378
90	8.63	1.24	2.15	4.65	0.675	8.74
120	4.42	0.334	2.07	4.17	0.492	5.99

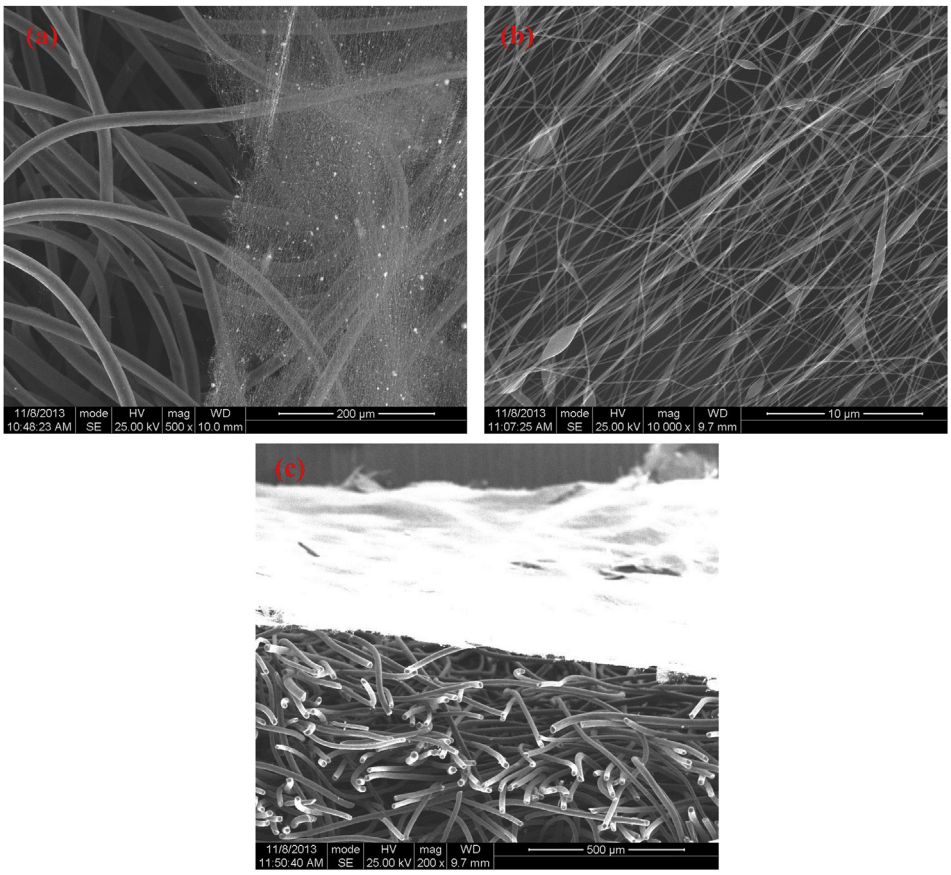

Fig. 13. SEM images of the ECW/CF composite electrode: (a) surface morphology of the composite electrode, (b) surface morphology of the ECW as catalyst layer, (c) cross-section of the composite electrode.

is larger than that of the pristine CF, which is ascribed to more active sites for the redox reaction provided by the ECW. The results mentioned above suggest the electrochemical activity of ECW is better than that of CF, which is consistent with the comparison result between ECW and CF in the previous work [14]. The relative explanation can be found in the article. Therefore, using the ECW as catalyst layer for CF electrode can improve latter electrochemical properties greatly.

3.5. Performance of VRFB single cell

As for ECW catalyst layer application, two methods were designed as mentioned above. For the first method, the performance of VRFB single cell with the ECW/CF composite electrode, pristine CF and 1000 °C-1.5 h CF have been tested in the symmetric cell firstly, which used the same type of electrodes in both half cells. In addition, the ECW/CF composite electrode was also tested in two kinds of asymmetric cells. For cell 1, the ECW/CF composite electrode served as positive electrode and the pristine CF served as negative one. This case is denoted as positive side. For cell 2, the ECW/CF composite electrode served as negative electrode and the pristine CF served as positive one. This case is denoted as negative side. The average efficiencies of the cell with different electrodes at a current density of 50 mA cm^{-2} are listed in Table 10.

Due to the better electrochemical performance of the ECW/CF composite electrode, coulombic efficiency (CE) of the cell with the composite electrode is higher than that of the cell with the pristine CF. The phenomenon is consistent with the previous work [33]. However, loss of function groups during the carbonization process may reduce the hydrophilicity of CF, which will enlarge the physical resistances of the battery. Therefore, voltage efficiencies (VE) for the symmetric cells with the 1000 °C-1.5 h CF and ECW/CF composite electrode are smaller than that of the cell with pristine CF. As for the asymmetric cell, positive side shows higher CE than the negative side. It indicates improvement of the cell performance mainly depends on the enhancement of the negative electrode, which corresponds to the CV results. Fig. 15 shows the charge capacity decrease of the single cell for the first 50 cycles. It can be seen clearly the capacity decrease of the cell with ECW/CF composite electrode is smaller than that with pristine CF, which may be attributed to the addition of the ECW on the CF. The relative mechanism needs further investigation. From the results mentioned above, VRFB single cell with the ECW/CF composite electrode shows higher CE and better capacity retention compared with the cell with the pristine CF. However, due to the increased physical resistances, EE of the cell with the ECW/CF composite electrode is slightly lower than that of the cell with the pristine CF.

To avoid increasing physical resistances of the cell and improve its EE, the 90 min-ECW was applied in VRFB single cell with the second method. The 90 min-ECW was sandwiched between CF electrode and ion exchange membrane as catalyst layer in both half cells during the single cell test. As it is predicted, the physical resistances of the cell with ECW are not larger than the cell without ECW. Fig. 16 shows average efficiencies of the cells with and without ECW at different current densities. Compared with the cell without ECW, CE of the cell with ECW is higher, which is similar to the test result using the first method. At the low charge current density, VE of the cell with ECW is a little higher than that of the cell

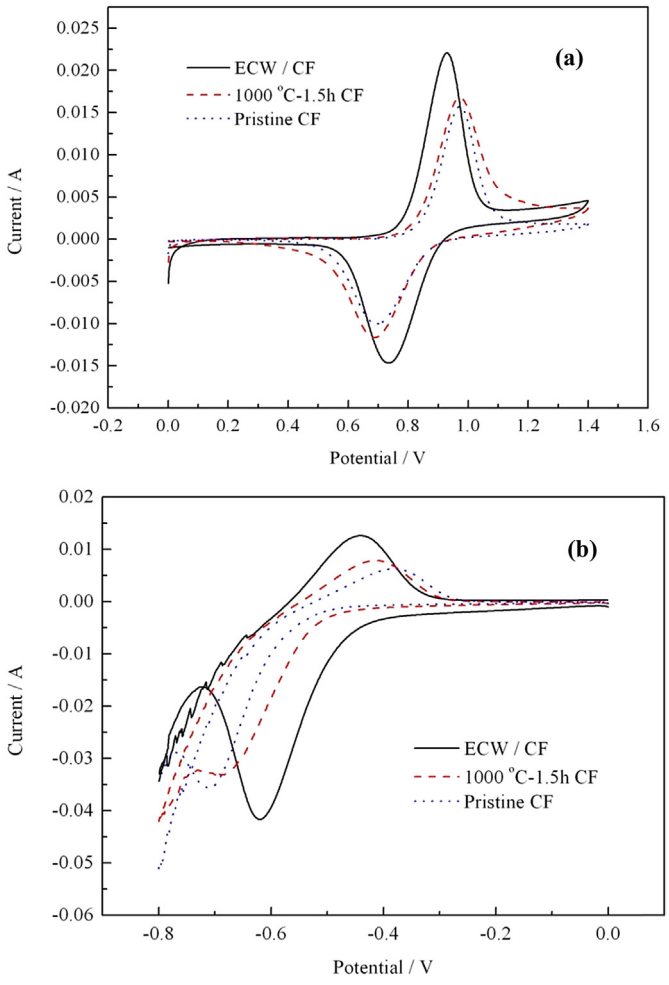

Fig. 14. CV curves for VO^{2+}/VO_2^+ (a) and V^{2+}/V^{3+} redox couple (b) on the pristine CF, 1000 °C-1.5 h CF, and ECW/CF composite electrode recorded at 2 mV s^{-1} scan rate in 0.1 M $VOSO_4$ + 2.0 M H_2SO_4.

Table 8
Parameters recorded by the CV curves for VO^{2+}/VO_2^+ couple on the pristine CF, 1000 °C-1.5 h CF, and ECW/CF composite electrode.

Samples	Ipa (mA)	Ipc (mA)	−Ipa/Ipc	Ea (V)	Ec (V)	ΔEp (V)
ECW/CF	22.1	14.8	1.49	0.928	0.736	0.192
1000 °C-1.5 h CF	16.8	11.7	1.44	0.973	0.687	0.286
Pristine CF	15.7	10	1.57	0.973	0.696	0.277

Table 9
Parameters recorded by the CV curves for V^{2+}/V^{3+} couple on the pristine CF, 1000 °C-1.5 h CF, and ECW/CF composite electrode.

Samples	Ipa (mA)	Ipc (mA)	−Ipa/Ipc	Ea (V)	Ec (V)	ΔEp (V)
ECW/CF	12.6	41.7	0.302	0.44	0.62	0.18
1000 °C-1.5 h CF	7.84	33.1	0.237	0.415	0.69	0.275
Pristine CF	6.39	35.6	0.179	0.381	0.714	0.333

Table 10
VRFB single cell efficiencies for different electrodes at a current density of 50 mA cm^{-2}.

Samples	CE/%	VE/%	EE/%
Pristine CF	93.8	89.3	83.8
1000 °C-1.5 h CF	94.1	87.3	82.2
ECW/CF	94.9	88.1	83.6
Positive side	94.4	87.5	82.6
Negative side	95.0	84.2	80.0

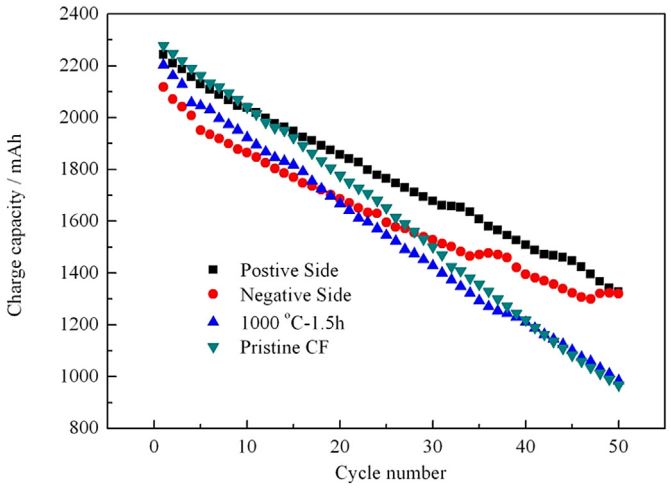

Fig. 15. Charge capacity decrease of the single cell with different electrodes at a current density of 50 mA cm^{-2}.

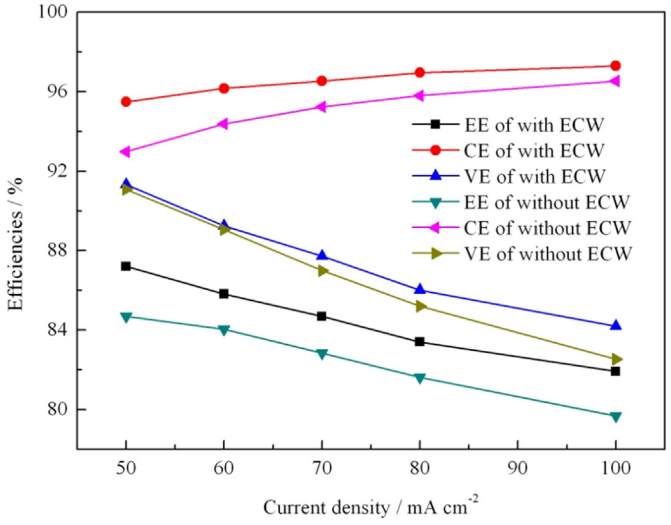

Fig. 16. Efficiencies of the VRFB single cell with and without ECW at different current densities.

without ECW. However, as the charge current density increases, the difference between VE for two electrodes increases. It may owe to the more important role of the ECW catalyst layer plays on reducing electrochemical polarization of the cell. As a result of the improvement of CE and VE mentioned above, EE of the cell with ECW is about 2% higher than that of the cell without ECW at all current densities. The relative parameters are listed in Table 11.

Fig. 17 shows charge–discharge curve of the VRFB single cell with and without ECW at a current density of 100 mA cm^{-2}. A reduced overpotential marked in the figure in both charge and discharge processes demonstrate the high electrochemical activity of the ECW catalyst layer. Due to the lower overpotential, the charge and discharge capacity of the cell with ECW are larger than that of the cell without ECW. Fig. 18 presents discharge capacity decrease of the single cell with and without ECW at different current densities. The cell with ECW shows better utilization of the electrolyte and capacity retention compared with the cell without ECW, which is also similar to the test result using the first method. Fig. 19 illustrates the EE of VRFB single cells with and without ECW at different current densities. Compared with the cell without ECW,

Table 11
VRFB single cell efficiencies with and without ECW at different current densities.

Current density/mA cm^{-2}	With ECW			Without ECW		
	CE/%	VE/%	EE/%	CE/%	VE/%	EE/%
50	95.5	91.3	87.2	93.0	91.1	84.7
60	96.2	89.2	85.8	94.4	89.0	84.0
70	96.5	87.7	84.7	95.2	87.0	82.8
80	97.0	86.0	83.4	95.8	85.2	81.6
100	97.3	84.2	81.9	96.5	82.5	79.7

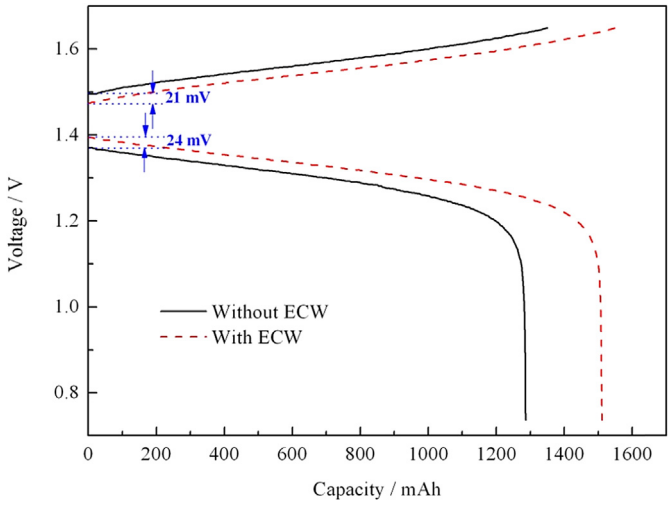

Fig. 17. Charge–discharge curve of the VRFB single cell with and without ECW at a current density of 100 mA cm^{-2}.

EE of the cell with ECW decreases a little at a current density of 50 mA cm^{-2} after testing for 90 cycles (about 189 h), suggesting the properties of ECW catalyst layer are stable. All in all, due to the high electrochemical properties of ECW catalyst layer, the cell performance was enhanced a lot.

In this paper, a rudimentary and efficient method to use the ECW as catalyst layer in VRFB has been proposed. The effect of loading capacity and thickness of ECW on the performance of ECW/CF composite electrode has not been studied yet. There is still a lot

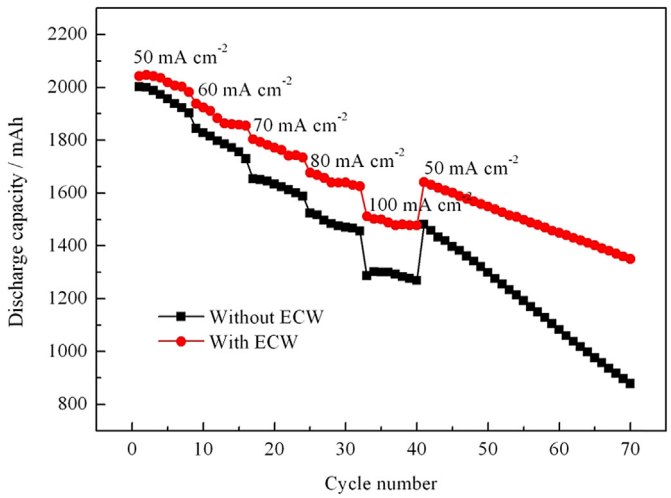

Fig. 18. Discharge capacity decrease of the single cell with and without ECW at different current densities.

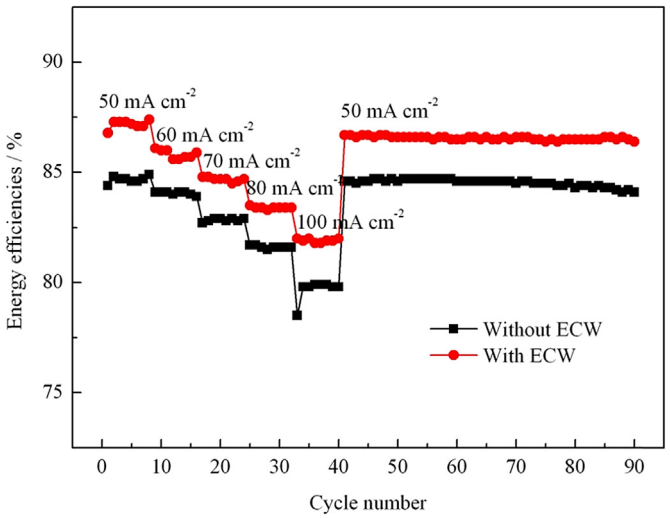

Fig. 19. EE of VRFB single cell with and without ECW at different current densities.

of work to do to optimize the electrochemical performance of the composite electrode. In the follow-on work, the electrocatalytic activity of ECW needs to be improved as well as the loading method of ECW on the pristine CF also needs to be optimized. With further enhancement of the electrochemical properties of ECW, it is believed that the cell with ECW as catalyst layer will present higher EE.

4. Conclusions

PAN-based ECW has been developed by electrospinning and subsequent carbonization process at 1000 °C for different times in this paper. With the increasing of carbonization time, the electrochemical reversibility of vanadium redox couples on the ECW is improved step by step. The increasing electrochemical activity of the ECW can be attributed to the promoted electron transfer rate and enhanced mass transport process, which results from the conversion of fibers carbon structure. Forming of the mountains of 2-dimensional graphitic lattices not only helps to improve the electrical conductivity of the fibers to facilitate the electron transfer, but also contributes to accelerate the mass transport. Edge planes of the graphitic lattice act as active sites for the vanadium redox reaction. Due to the high electrochemical activity of ECW toward the vanadium redox reaction, the performance of VRFB applying the 90 min-ECW as catalyst layer is enhanced remarkably.

Acknowledgments

This work is funded by National Basic Research Program of China (No. 2010CB227203).

References

[1] A. Poullikkas, Renew. Sustain. Energy Rev. 27 (2013) 778–788.
[2] G. Kear, A.A. Shah, F.C. Walsh, Int. J. Energy Res. 36 (2012) 1105–1120.
[3] A. Parasuraman, T.M. Lim, C. Menictas, M. Skyllas-Kazacos, Electrochim. Acta 101 (2013) 27–40.
[4] M. Skyllas-Kazacos, M. Rychcik, R.G. Robins, A.G. Fane, M.A. Green, J. Electrochem. Soc. (1986) 1057–1058.
[5] P. Alotto, M. Guarnieri, F. Moro, Renew. Sustain. Energy Rev. 29 (2014) 325–335.
[6] B. Sun, M. Skyllas-Kazacos, Electrochim. Acta 37 (1992) 1253–1260.
[7] B. Sun, M. Skyllas-Kazacos, Electrochim. Acta 37 (1992) 2459–2465.
[8] W.H. Wang, X.D. Wang, Electrochim. Acta 52 (2007) 6755–6762.
[9] B. Li, M. Gu, Z. Nie, Y. Shao, Q. Luo, X. Wei, et al., Nano Lett. 13 (2013) 1330–1335.

[10] Z.M. Huang, Y.Z. Zhang, M. Kotaki, S. Ramakrishna, Compos. Sci. Technol. 63 (2003) 2223–2253.
[11] M.J. Laudenslager, R.H. Scheffler, W.M. Sigmund, Pure Appl. Chem. 82 (2010) 2137–2156.
[12] Y. Yang, F. Simeon, T.A. Hatton, G.C. Rutledge, J. Appl. Polym. Sci. 124 (2012) 3861–3870.
[13] S.N. Arshad, M. Naraghi, I. Chasiotis, Carbon 49 (2011) 1710–1719.
[14] G. Wei, J. Liu, H. Zhao, C. Yan, J. Power Sources 241 (2013) 709–717.
[15] J.R. Pels, F. Kapteijn, J.A. Moulijn, et al., Carbon 33 (1995) 1641–1653.
[16] C. Weidenthaler, A.H. Lu, W. Schmidt, F. Schüth, Microporous Mesoporous Mater. 88 (2006) 238–243.
[17] L. Yue, W. Li, F. Sun, L. Zhao, L. Xing, Carbon 48 (2010) 3079–3090.
[18] K.J. Kim, Y.J. Kim, J.H. Kim, M.S. Park, Mater. Chem. Phys. 131 (2011) 547–553.
[19] B.S. Lee, S.B. Son, K.M. Park, W.R. Yu, K.H. Oh, S.H. Lee, J. Power Sources 199 (2012) 53–60.
[20] W. Xie, H.F. Cheng, Z.Y. Chu, Z.H. Chen, Ceram. Int. 35 (2009) 2705–2710.
[21] E. Zussman, X. Chen, W. Ding, L. Calabri, D.A. Dikin, J.P. Quintana, et al., Carbon 43 (2005) 2175–2185.
[22] Y. Qiu, J. Yu, T. Shi, X. Zhou, X. Bai, J.Y. Huang, J. Power Sources 196 (2011) 9862–9867.
[23] K. Kinoshita, Carbon Electrochemical and Physicochemical Properties, Wiley, 1988.
[24] Z. González, C. Botas, P. Álvarez, S. Roldán, C. Blanco, R. Santamaría, et al., Carbon 50 (2012) 828–834.
[25] P. Han, H. Wang, Z. Liu, X. Chen, W. Ma, J. Yao, et al., Carbon 49 (2011) 693–700.
[26] A.J. Bard, L.R. Faulkner, Electrochemical Methods Fundamentals and Applications, second ed., Wiley, 2001.
[27] H.M. Tsai, S.Y. Yang, C.M. Ma, X. Xie, Electroanalysis 23 (2011) 2139–2143.
[28] J. Jin, X. Fu, Q. Liu, et al., ACS Nano 7 (2013) 4764–4773.
[29] C. Kim, K.S. Yang, Appl. Phys. Lett. 83 (2003) 1216–1218.
[30] M. Park, Y.-j. Jung, J. Kim, Hi. Lee, J. Cho, Nano Lett. 13 (2013) 4833–4839.
[31] S. De Fonton, A. Oberlin, M. Inagaki, J. Mater. Sci. 15 (1980) 909–917.
[32] C.E. Banks, T.J. Davies, G.G. Wildgoose, R.G. Compton, Chem. Commun. (2005) 829–841.
[33] G. Wei, C. Jia, J. Liu, C. Yan, J. Power Sources 220 (2012) 185–192.